Advanced Journal of Chemistry-Section A, 2020, *3*, S740–S749 (*Special Issue*)
Available online at : www.ajchem-a.com
ISSN Online: 2645-5676
DOI: 10.22034/AJCA.2020.107642

Original Research Article

Nalidixic Acid Adsorption on the Surface of Boron Nitride Nanocluster ($B_{12}N_{12}$): DFT Studies

Mohammad Reza Jalali Sarvestani [a,*], Zohreh Doroudi [b]

[a] *Young Researchers and Elite Club, Yadegar-e-Imam Khomeini (RAH) Shahr-e-Rey Branch, Islamic Azad University, Tehran, Iran*
[b] *Department of Chemistry, Yadegar-e-Imam Khomeini (RAH) Shahre-Rey Branch, Islamic Azad University, Tehran, Iran*

ARTICLE INFO

Received: 28 April 2020
Revised: 16 May 2020
Accepted: 19 May 2020
Available online: 21 May 2020

KEYWORDS

Nalidixic acid
$B_{12}N_{12}$
Adsorption
NBO
DFT
Sensor

ABSTRACT

In this research study, the detection and removal of nalidixic acid by boron nitride nanocluster ($B_{12}N_{12}$) were investigated using the DFT, infra-red (IR), natural bond orbital (NBO) and frontier molecular orbital (FMO) computations. The calculated negative values of adsorption energy, Gibbs free energy changes, and great amounts of thermodynamic equilibrium constants demonstrated nalidixic acid adsorption on the surface of $B_{12}N_{12}$ was spontaneous, irreversible and experimentally feasible. The values of adsorption enthalpy changes and specific heat capacity (C_V) revealed that, the interaction of the adsorbate and adsorbent was exothermic and $B_{12}N_{12}$ was an ideal nanostructure for the construction of new thermal sensors for detection of nalidixic acid. The influence of temperature on the thermodynamic parameters was also investigated and the results demonstrated that, the adsorption process was more favorable at room temperature. The NBO results indicated in all of the studied configurations covalent bonds were formed between nalidixic acid and $B_{12}N_{12}$ and their interaction was chemisorption. The density of states (DOS) spectrums showed that, the bandgap of boron nitride nanocage after the adsorption of nalidixic acid decreased from 14.864 (eV) to 7.314 (eV), indicating that the electrical conductivity of $B_{12}N_{12}$ improved significantly in the adsorption process and $B_{12}N_{12}$ is an appropriate sensing material for developing novel electrochemical sensor to nalidixic acid determination. The important structural parameters including chemical hardness, chemical potential, dipole moment, electrophilicity and maximum charge capacity were also computed and discussed in detail.

GRAPHICAL ABSTRACT

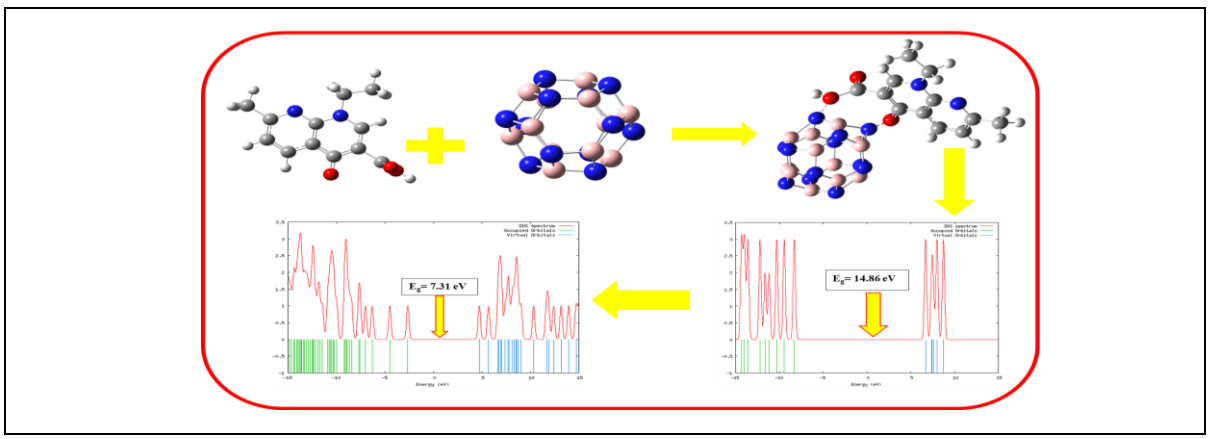

* Corresponding author's E-mail address: rezajalali93@yahoo.com

Introduction

In the last few years, pharmaceuticals have caused a growing concern due to their presence in environmental samples. Among these compounds, it should be highlighted that, the antibiotics which are used in large quantities for several decades as human infection medicine, veterinary medicine, and husbandry growth promoters. Due to incomplete metabolization of these compounds in human and animal body, a portion of administered antibiotic is excreted as the parent compound or as metabolites via urine and feces. As a result of the agricultural application of manure and sewage sludge containing unmetabolized drugs, wastewater irrigation, and the disposal of domestic and hospital waste, they are eventually released into soils, sediments, and aquatic environments through different pathways [1–3].

Nalidixic acid (NA) (1-ethyl-1,4-dihydro-7-methyl-4-oxo-1,8-naphthyridine-3-carboxylic acid), as shown in Figure 1, is the first synthetic quinolone antibiotic that was introduced in therapy in the 1960s [4]. NA is effective against both gram-positive and gram-negative microbes. It acts as a bacteriostatic agent in lower concentrations, but can be bactericidal at higher concentrations. Nalidixic acid has been selected in the present study because of its presence in hospital wastes, wastewater treatment plants effluents, environmental waters and soils [5-7]. It has serious effects on human health, such as chronic toxicity and carcinogenicity effect [8]. Various methods for removing nalidixic acid from aqueous solutions were used, including an embedded MBR-ozonation scheme [9], powdered activated carbon [10], adsorption onto anion-exchange and neutral polymers [11] and UV and UV/H_2O_2 processes [12]. Adsorption, as a simple and relatively economic method, is widely utilized in the removal of pollutants.

Boron nitrides (BN) are constructed from equal numbers of boron (B) and nitrogen (N) atoms. Balmain *et al*. [13,14] first demonstrated the synthesis of BN in 1842 by using the reaction between molten H_3BO_3 and potassium cyanide (KCN). Since then, an enormous amount of investigations has been carried out on the preparation of various BN nanostructures including nanocages, nanotubes, nanosheets, and nanoporous frameworks. These nanostructures exhibited excellent physical and chemical properties, such as high specific surface area (SSA), electrical insulation, wide energy band gap, high thermal stability and conductivity, ultraviolet photoluminescence, and superb resistance to oxidation as well as the chemical inertness [15-17].

Boron nitride nanomaterials exhibited different desirable physical and chemical properties in comparison to their carbon counterparts. Recently fullerene-like cage of boron nitride nanostructures have attracted considerable attention due to their remarkable chemical and physical properties, particularly of wide gap semiconductors [18–20]. The geometries and stability of fullerene-like $(BN)_n$ nanoclusters have been theoretically investigated by many researchers [21–23]. The $B_{12}N_{12}$ nanocluster is energetically the most stable cluster among different types of $(BN)_n$ structures. Figure 1 shows the optimized structure of the $B_{12}N_{12}$ nanocage [24-25]. The identification and removal of pollutants from the environment using $B_{12}N_{12}$ nanocage has been a subject of extensive studies [26-30]. In this respect, the performance of $B_{12}N_{12}$ as an adsorbent and sensing material for detection and removal of Nalidixic acid was evaluated using the DFT, NBO, IR, and FMO computations for the first time in this research.

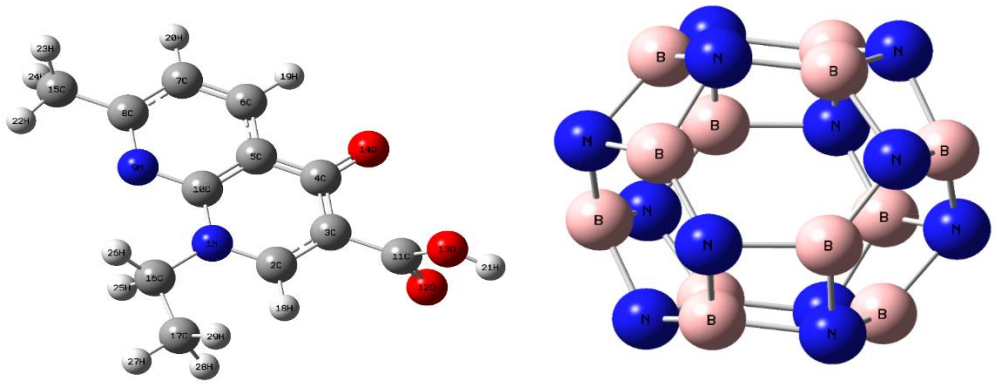

NA **Boron Nitride Nanocluster ($B_{12}N_{12}$)**

Figure 1. Optimized structures of NA and BN nanocage

Experimental

Computational details

The structures of $B_{12}N_{12}$, NA and their complexes were drawn up by Nanotube modeler 1.3.0.3 and Guass View 6 software [31,32]. Firstly, all of the designed structures were optimized geometrically. Then, IR, NBO, and FMO computations were performed. All of the computations were conducted by Gaussian 16 software using the density functional theory method in the B3LYP/6-31G (d) level of theory [33-34]. All of the computations were performed in the aqueous phase at 298-398 at 10˚ intervals.

The studied processes were as follows:

$$NA + B12N12 \longrightarrow NA\text{-}B12N12 \quad (1)$$

Equations 2-6 were used to calculate the adsorption energy values (E_{ad}) and thermodynamic parameters including, the adsorption enthalpy changes (ΔH_{ad}), Gibbs free energy changes (ΔG_{ad}) thermodynamic equilibrium constants (K_{th}), and entropy changes (ΔS_{ad}) respectively [23-25].

$$E_{ad} = \left(E_{(\text{NA-B12N12})} - \left(E_{(\text{NA})} + E_{(B12N12)}\right)\right) \quad (2)$$

$$\Delta H_{ad} = \left(H_{(\text{NA-B12N12})} - \left(H_{(\text{NA})} + H_{(B12N12)}\right)\right) \quad (3)$$

$$\Delta G_{ad} = \left(G_{(\text{NA-B12N12})} - \left(G_{(\text{NA})} + G_{(B12N12)}\right)\right) \quad (4)$$

$$K_{th} = \exp\left(-\frac{\Delta G_{ad}}{RT}\right) \quad (5)$$

$$\Delta S_{ad} = \left(S_{(\text{NA-B12N12})} - \left(S_{(\text{NA})} + S_{(B12N12)}\right)\right) \quad (6)$$

In the aforementioned equations, E is the total electronic energy of each structure, H denotes the sum of the thermal correction of enthalpy and total energy of the evaluated materials. The G stands for the sum of the thermal correction of Gibbs free energy and total energy for each of the studied structures. R denotes the ideal gas constants, T is the temperature and S stands for the thermal correction of entropy for each structure [26].

Frontier molecular orbital parameters including bandgap (E_g), chemical hardness (η), chemical potential (μ), electrophilicity (ω) and the maximum charge capacity (ΔN_{max}) were calculated using the Equations 7-11 [27].

$$Eg = E_{LUMO} - E_{HOMO} \quad (7)$$

$$\eta = {}^{(E_{LUMO} - E_{HOMO})}/_{2} \quad (8)$$

$$\mu = {}^{(E_{LUMO} + E_{HOMO})}/_{2} \quad (9)$$

$$\omega = {}^{\mu^2}/_{2\eta} \quad (10)$$

$$\Delta N_{max} = -{}^{\mu}/_{\eta} \quad (11)$$

E_{LUMO} and E_{HOMO} in the Equations 7 to 11, are the energy of the lowest unoccupied molecular orbital and the energy of the highest occupied molecular orbital respectively [27].

Results and discussion

NBO and structural analysis

As seen in Figure 2, the interaction of NA with $B_{12}N_{12}$ was studied in three different situations to find the most stable configuration. In A-Conformer, the NA molecule is approached to the surface of the nanostructure towards its methyl group. In B-Conformer, the aromatic rings of NA are inserted near the surface of $B_{12}N_{12}$ in parallel form. In C-Conformer, the medicine is oriented to the surface of boron nitride nanocage from its carbonyl and carboxylic acid functional groups. As can be seen in Figure 2, in all of the configurations, sharp deformations in the structure of $B_{12}N_{12}$ near the interacting sites are distinguishable in the optimized structures. This phenomenon indicated that, some chemical bonds were formed between the NA and the nano-adsorbent [23]. In this respect, to obtain more information about the adsorption mechanism and also the nature of interactions NBO computations were performed on all of the structures and (Table 1). As seen in Table 2, at B and C configurations two monovalent bonds are formed between the adsorbent and the adsorbate. While in the case of A-Conformer only one bivalent bond with SP^2 hybridization is created between NA and $B_{12}N_{12}$. Therefore, NA interaction with BN nanocluster is chemisorption in all of the conformers [24]. For gaining more insights about the adsorption process, the values of total electronic energy and adsorption energy were also calculated (Table 2). The adsorption energy value for all of the conformers is highly negative which indicated that, the adsorption process was experimentally possible at all of the positions. Among the studied configurations, C-Conformer is the most stable one and the interaction process is more favorable in this situation because the total electronic energy and adsorption energy values of this conformer are more negative than other ones [25].

Table 1. The calculated values of adsorption energy, total electronic energy, the lowest frequency, zero-point energy, bond energy, hybridization, occupancy, bond order and bondlenghts

		Zero-point energy (kJ/mol)	The lowest frequency (cm^{-1})	Adsorption energy (kJ/mol)	Total electronic energy (a.u)	Bond energy (a.u.)	Hybridization	Occupancy	Bond order	Bond length (Å)
NA	---	---	---	---	---	---	-784.860	---	36.091	689.680
$B_{12}N_{12}$	---	---	---	---	---	---	-938.547	---	369.919	391.630
A-Conformer	C_{17}-N	1.42	2	4.01	$Sp^{2.01}$	-0.512	-1723.502	-250.743	5.142	1082.350
B-Conformer	C_{10}-N	1.58	1	1.98	$Sp^{2.96}$	-0.265	-1723.463	-148.648	9.921	1089.08
	C_{10}-B	1.67	1	2.01	$Sp^{2.99}$	-0.199				
C-Conformer	O_{13}-N	1.71	1	2.02	$Sp^{2.97}$	-0.350	-1723.633	-596.217	6.460	1084.110
	O_{14}-N	1.63	1	1.96	$Sp^{3.01}$	-0.441				

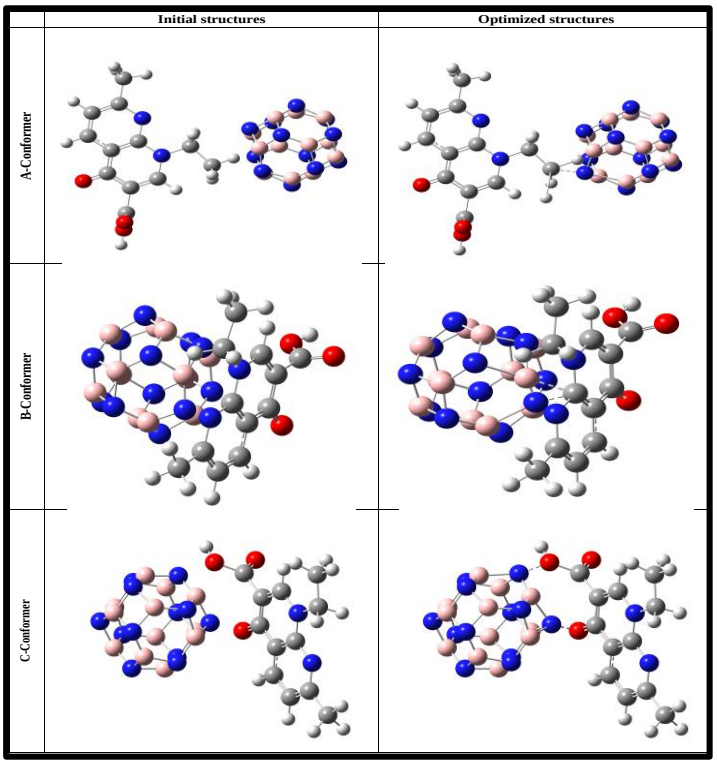

Figure 2. Initial and optimized structures of NA-$B_{12}N_{12}$ complexes

Thermodynamic studies

The calculated values of the enthalpy changes and specific heat capacity are presented in Table 2. As can be seen, the NA interaction with BN nanocage is exothermic at all of the evaluated configurations as the ΔH_{ad} values are negative for all of the conformers. The effect of temperature on this parameter was also checked out; however, by increasing the temperature no tangible change occurred in the values of ΔH_{ad}. Therefore, the optimum temperature for the NA adsorption process cannot be determined based on this parameter [26]. The C_V values for both the $B_{12}N_{12}$ and NA increased remarkably when NA is adsorbed on the surface of BN nanocage, indicating that the thermal conductivity of the nanostructure and medicine enhanced significantly after their interaction. Therefore, the BN nanocluster is an excellent sensing material for the fabrication of new NA thermal sensors. In thermal sensors, the desired analyte participates in a reaction with the recognition element of the sensor and their interaction should be highly exothermic or endothermic. Also, the variations in the temperature should be recorded by a thermistor and will be used as a signal which has a direct relationship with the analyte concentration. Since NA interaction with $B_{12}N_{12}$ is exothermic and the thermal conductivity of the nano-adsorbent enhanced in the adsorption process, it seems that, the BN nanocage can be used for thermal detection of the NA [24].

The computed values of the Gibbs free energy changes and thermodynamic equilibrium constants are presented in Table 3. The adsorption of the NA at all of the conformers is spontaneous, non-equilibrium and irreversible as the calculated ΔG_{ad} and K_{th} values are highly negative and positive, respectively. The influence of temperature on both parameters was also assessed. As can be seen, by increasing the temperature, the values of ΔG_{ad} became more positive and the values of K_{th} approached to zero. Therefore, the NA interaction with BN nanocluster was more favorable in the lower temperatures [27].

Table 2. The calculated enthalpy changes (ΔH_{ad}) and specific heat capacity (C_V) in the temperature range of 298-398 K at 10˚ intervals

Temperature (K)	ΔH_{ad} (kJ/mol)			C_V (J/mol.K)			$B_{12}N_{12}$	NA
	A-Conformer	B-Conformer	C-Conformer	A-Conformer	B-Conformer	C-Conformer		
298	-252.213	-144.494	-592.306	423.797	416.743	416.972	177.536	221.603
308	-252.285	-144.595	-592.399	438.128	431.305	431.538	185.935	227.523
318	-252.369	-144.697	-592.500	452.364	445.766	446.004	194.259	233.423
328	-252.453	-144.797	-592.598	466.488	460.112	460.355	202.497	239.300
338	-252.537	-144.895	-592.695	480.487	474.328	474.574	210.635	245.151
348	-252.621	-144.992	-592.789	494.347	488.399	488.648	218.665	250.972
358	-252.705	-145.087	-592.882	508.055	502.314	502.565	226.577	256.760
368	-252.787	-145.164	-592.959	521.600	516.060	516.314	234.364	262.512
378	-252.870	-145.224	-593.022	534.973	529.628	529.884	242.019	268.224
388	-252.954	-145.310	-593.109	548.165	543.008	543.265	249.536	273.892
398	-253.038	-145.397	-593.194	561.167	556.193	556.451	256.912	279.512

Table 3. The calculated Gibbs free energy changes (ΔG_{ad}) and thermodynamic constants (K_{th}) in the temperature range of 298-398 K at 10˚ intervals

Temperature (K)	ΔG_{ad} (kJ/mol)			K_{th}		
	A-Conformer	B-Conformer	C-Conformer	A-Conformer	B-Conformer	C-Conformer
298	-182.189	-71.348	-519.237	$8.315\times10^{+31}$	$3.165\times10^{+12}$	$9.363\times10^{+90}$
308	-179.576	-68.769	-516.591	$2.761\times10^{+30}$	$4.545\times10^{+11}$	$3.721\times10^{+87}$
318	-176.960	-66.140	-513.917	$1.134\times10^{+29}$	$7.234\times10^{+10}$	$2.394\times10^{+84}$
328	-174.334	-63.457	-511.233	$5.640\times10^{+27}$	$1.263\times10^{+10}$	$2.402\times10^{+81}$
338	-171.697	-60.764	-508.539	$3.337\times10^{+26}$	$2.436\times10^{+09}$	$3.613\times10^{+78}$
348	-169.061	-58.064	-505.826	$2.323\times10^{+25}$	$5.151\times10^{+08}$	$7.840\times10^{+75}$
358	-166.406	-55.354	-503.115	$1.864\times10^{+24}$	$1.184\times10^{+08}$	$2.398\times10^{+73}$
368	-163.776	-52.628	-500.409	$1.730\times10^{+23}$	$2.933\times10^{+07}$	$1.006\times10^{+71}$
378	-161.104	-49.869	-497.655	$1.796\times10^{+22}$	$7.741\times10^{+06}$	$5.554\times10^{+68}$
388	-158.422	-47.131	-494.920	$2.090\times10^{+21}$	$2.202\times10^{+06}$	$4.031\times10^{+66}$
398	-155.732	-44.389	-492.177	$2.702\times10^{+20}$	$6.664\times10^{+05}$	$3.738\times10^{+64}$

The calculated adsorption entropy changes are tabulated in Table 4. As the presented data revealed clearly, the randomness and chaos decreased sharply when NA adsorbs on the surface of $B_{12}N_{12}$ as the computed ΔS_{ad} values were negative for all of the investigated conformers. The ΔS_{ad} is usually negative for the adsorption systems in which the adsorbate molecules aggregated with the adsorbent [26].

FMO analysis

The difference between the energies of HOMO and LUMO orbitals is known as bandgap and this parameter has a direct relationship with the electrical conductivity of compounds. In fact, the molecules with low bandgap are more conductive than the compounds with large bandgap. For evaluating this parameter, the DOS spectrums of BN nanocage and its complexes with NA were computed and the obtained spectrums were presented in Figure 3. As can be seen, the E_g of the nanostructure is 14.864 (eV) but when NA adsorbs on its surface the bandgap decreases to 10.828 (eV) for A-Conformer and in the case of B and C conformers it decreases to 7.314 and 7.690 eV [24-26]. This phenomenon shows the electrical conductivity of $B_{12}N_{12}$ improved significantly after the adsorption of NA on its surface and this nanomaterial can be used as a sensing material in the development of new electrochemical sensors for detection of NA [27].

The values of chemical hardness and chemical potential were calculated by Equations 8 and 9 and the results were given in Table 5. The molecules with a low amount of chemical hardness and high values of chemical potential are more reactive than other compounds [23]. As the provided data in Table 5 reveal obviously when NA adsorbs on the surface of $B_{12}N_{12}$ the chemical hardness experience a tangible decrease but the chemical potential increases acutely. Therefore, it can be inferred that the reactivity of NA enhances after its interaction by boron nitride nanocage [25].

Electrophilicity and maximum charge capacity were the next evaluated parameters. When two molecules interact with each other one of them play the role of an electron donor and the other one play the role of electron acceptor. Molecules with high values of electrophilicity and low amounts of maximum transferred charge have more tendency to absorb electron than other compounds [26]. As the presented results in Table 5 show obviously, when NA adsorbs on the surface of nanostructure the electrophilicity decreases in A-Conformer but increases in the case of B and C conformers. Therefore, A-Conformer has a lower tendency towards electrons while B and C conformers are more electrophile than pure NA without nano-adsorbent. The dipole moment was the last evaluated parameter. As can be seen from Table 5, the dipole moments of NA complexes with $B_{12}N_{12}$ are higher than the dipole moment of NA. Hence, NA complexes with BN nanocage has better solubility in water than pure NA [23].

Table 4. The calculated entropy changes (ΔS_{ad}) in the temperature range of 298-398 K at 10˚ intervals

Temperature (K)	ΔS_{ad} (J/mol.K) A-Conformer	B-Conformer	C-Conformer
298	-234.980	-245.455	-245.198
308	-236.068	-246.189	-246.131
318	-237.135	-247.036	-247.116
328	-238.168	-247.989	-248.065
338	-239.170	-248.909	-248.979
348	-240.113	-249.793	-249.894
358	-241.057	-250.649	-250.746
368	-241.875	-251.458	-251.496
378	-242.769	-252.260	-252.293
388	-243.640	-253.037	-253.064
398	-244.488	-253.790	-253.812

Table 5. The calculated energies of HOMO and LUMO, bandgap, chemical hardness, chemical potential, electrophilicity, maximum charge capacity and dipole moment

	E_H (eV)	E_L (eV)	E_g (eV)	η (eV)	μ (eV)	ω (eV)	ΔN_{max} (eV)	Dipole moment (Deby)
NA	-5.821	5.066	10.887	5.443	-0.377	0.013	0.069	3.260
$B_{12}N_{12}$	-8.229	6.635	14.864	7.432	-0.797	0.043	0.107	0.000
A-Conformer	-5.574	5.254	10.828	5.414	-0.160	0.002	0.030	4.480
B-Conformer	-2.62	4.69	7.314	3.657	1.032	0.146	-0.282	7.190
C-Conformer	-2.521	5.169	7.690	3.845	1.324	0.228	-0.344	7.500

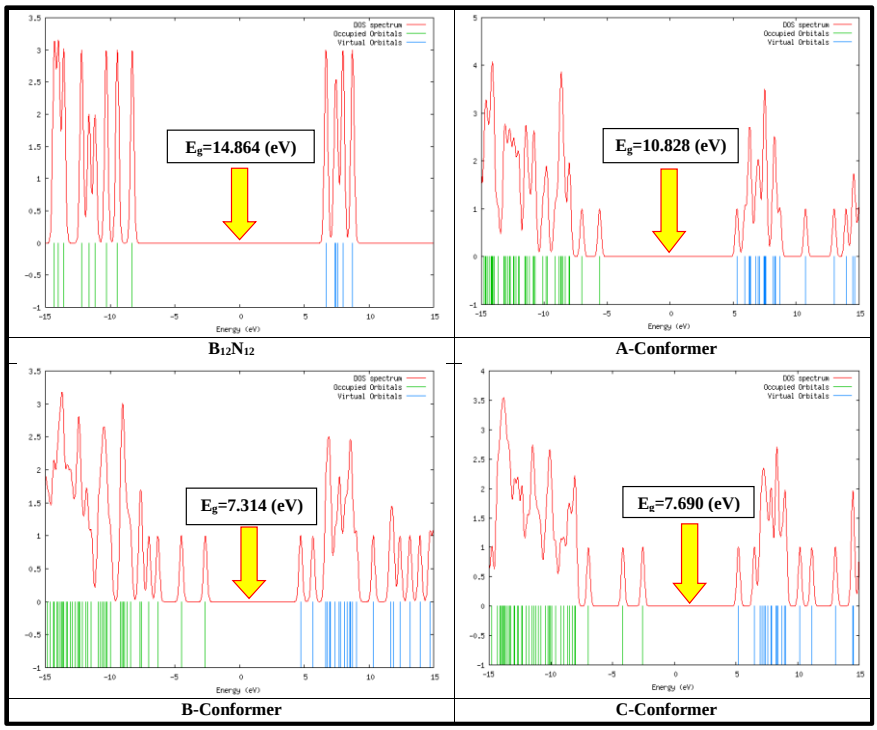

Figure 3. DOS spectrums of $B_{12}N_{12}$ and its complexes with NA

Conclusion

Removal and detection of NA is of great importance. On the other hand, boron nitride nanocluster has prominent features that make it a good candidate as an adsorbent and a sensing material for removal and sensing of different molecules. In this respect, NA adsorption on the surface of $B_{12}N_{12}$ was evaluated in this research by DFT, NBO and FMO computations. The calculated thermodynamic parameters demonstrated that, the NA interaction with $B_{12}N_{12}$ was exothermic, spontaneous, non-equilibrium, irreversible and the randomness decreased in the adsorption process. The specific heat capacity values demonstrated that, the thermal conductivity of the nanostructure enhanced substantially and $B_{12}N_{12}$ was found to be an excellent thermal sensing material for NA. The NBO results showed that, the NA interaction with the adsorbent was chemisorption and covalent bonds were formed between the NA and BN nanocage in all of the configurations. The DOS spectrums demonstrated that, the conductivity and electrocatalytic behavior of $B_{12}N_{12}$ improved remarkably in the adsorption process and this nanostructure was found to be an appropriate sensing material for the construction of new sensitive NA electrochemical sensors. The values of dipole moment, chemical hardness and chemical potential showed that, the solubility and reactivity of the NA improved when it was adsorbed on the surface of BN nanocage.

Acknowledgment

The authors would like acknowledge the young researchers and elite club of Islamic Azad University of Yadegar-e-Imam Khomeini (RAH) Shahre-rey branch for supporting this project.

Disclosure statement

No potential conflict of interest was reported by the authors.

References

[1] J.C. Leyva-Díaz, R.A. Phonbun, J. Taggart, E. Díaz, S. Ordonez, *Chemosphere.* **2019**, *218*, 128–137.

[2] L. Tahrani, L. Soufi, I. Mehri, A. Najjari, A. Hassan, J.V. Loco, T. Reyns, A. Cherif, H.B. Mansour, *Microb. Pathog.*, **2015**, *89*, 54–61.
[3] Q. Wu, Z. Li, H. Hong, *Appl. Clay Sci.*, **2013**, *74*, 66–73.
[4] P.M. de la Torre, Y. Enobakhare, G. Torrado, S. Torrado, *Biomaterials*, **2003**, *24*, 1499–1506.
[5] A.Y.C. Lin, T.H. Yu, C.F. Lin, *Chemosphere,* **2008**, *74*, 131–141.
[6] F. Tamtam, F. Van Oort, B. Le Bot, T. Dinh, S. Mompleat, M. Chevreuil, I. Lamy, M. Thiry, *Sci. Total Environ*., **2011**, *409*, 540–547.
[7] A.J. Watkinson, E.J. Murby, D.W. Kolpin, S.D. Costanzo, *Sci. Total Environ*., **2009**, *407*, 2711–2723.
[8] R.E. Morrissey, S. Eustis, J.K. Haseman, J. Huff, J.R. Bucher, *Drug Chem. Toxicol.,* **1991**, *14*, 45–66.
[9]. A. Pollice, G. Laera, D. Cassano, S. Diomede, A. Pinto, A. Lopez, G. Mascolo, *J. Hazard. Mater*., **2012**, *203-204*, 46–52.
[10] K.J. Choi, S.G. Kim, S.H. Kim, *Environ. Technol*., **2008**, *29*, 333–342.
[11] K.A. Robberson, A.B. Waghe, D.A. Sabatini, E.C. Butler, *Chemosphere*, **2006**, *63*, 934–941.
[12] I. Kim, N. Yamashita, H. Tanaka, *J. Hazard. Mater.*, **2009**, *166*, 1134–1140.
[13] W. Balmain, *Philos. Mag. Ser*., **1842**, *21*, 270–277.
[14] W. Balmain, *Philos. Adv. Synth*. *Catal*., **1842**, *27*, 422–430.
[15] S. Yu, Xi. Wang, H. Pang, R.i Zhang, W. Song, D. Fu, T. Hayat, X. Wang, *Chem. Eng. J*., **2018**, *333*, 343–360.
[16] S. Yourdkhani, T. Korona, N.L. Hadipour, *J. Phys. Chem*., **2015**, *11*, 6446–6467.
[17] E. Shakerzadeh, N. Barazesh, S.Z. Talebi, *Superlattice. Microst*., **2014**, 76, 264–276.
[18] M.T. Baei, *Comput. Theor. Chem*., **2013**, *1024*, 28–33.
[19] E. Shakerzadeh, E. Tahmasebi, Z. Biglari, *J. Mol. Liq*., **2016**, *221*, 443–451.
[20] A. Ahmadi Peyghan, H. Soleymanabadi, *Curr. Sci*., **2015**, *108*, 1910–1914.
[21] L. Mahdavian, *Russ. J. Appl. Chem.,* **2016**, *89*, 1528–1535.
[22] J. Beheshtiana, M. Kamfi Roozi, Z. Bagheri, A. Ahmadi Peyghan, *Chin. J. Chem. Phys*., **2012**, *25*, 60–64.
[23] M.R. Jalali Sarvestani, M. Gholizadeh Arashti, B. Mohasseb, *Int. J. New. Chem*., **2020**, *7*, 87–100.
[24] M.R. Jalali Sarvestani, R. Ahmadi, *Chem. Method*., **2020**, *4*, 40–54.
[25] M.R. Jalali Sarvestani, T. Boroushaki, M. Ezzati, *Int. J. New. Chem*., **2018**, *5*, 427–434.
[26] R. Ahmadi, M.R. Jalali Sarvestani, *Iran. Chem. Commun.*, **2019**, *7*, 344–351.
[27] M. Godarzi, R. Ahmadi, R. Ghiasi, M. Yousefi, *Int. J. Nano. Dimens.*, **2019**, *10*, 62–68.
[28] M.J. Islam, A. Kumer, N. Sarker, S. Paul, A. Zannat, *Adv. J. Chem. A.*, **2019**, *2*, 316–326.
[29] Z. Javanshir, S. Jameh-Bozorgi, P. Peyki, *Adv. J. Chem. A.*, **2018**, *1*, 117–126.
[30] M. Rezaei-Sameti, M. Jafari, *Chem. Method.*, **2020**, *4*, 494–513.
[31] Nanotube Modeler J. Crystal. Soft., **2014** software.
[32] R. Dennington, GaussView, Version 6.1, Todd A. Keith, and John M. Millam, Semichem Inc., Shawnee Mission, KS, **2016**.
[33] Gaussian 16, Revision C. 01, M.J. Frisch, G.W. Trucks, H.B. Schlegel, G.E. Scuseria, M.A. Robb, J.R. Cheeseman, G. Scalmani, V. Barone, G.A. Petersson, H. Nakatsuji, X. Li, M. Caricato, A.V. Marenich, J. Bloino, B.G. Janesko, R. Gomperts, B. Mennucci, H.P. Hratchian, J.V. Ortiz, A.F. Izmaylov, J.L. Sonnenberg, D. Williams-Young, F. Ding, F. Lipparini, F. Egidi, J. Goings, B. Peng, A. Petrone, T. Henderson, D. Ranasinghe, V.G. Zakrzewski, J. Gao, N. Rega, G. Zheng, W. Liang, M. Hada, M. Ehara, K. Toyota, R. Fukuda, J. Hasegawa, M. Ishida, T. Nakajima, Y. Honda, O. Kitao, H. Nakai, T. Vreven, K. Throssell, J.A. Montgomery, Jr.,

J.E. Peralta, F. Ogliaro, M.J. Bearpark, J.J. Heyd, E.N. Brothers, K.N. Kudin, V.N. Staroverov, T.A. Keith, R. Kobayashi, J. Normand, K. Raghavachari, A.P. Rendell, J.C. Burant, S.S. Iyengar, J. Tomasi, M. Cossi, J.M. Millam, M. Klene, C. Adamo, R. Cammi, J.W. Ochterski, R.L. Martin, K. Morokuma, O. Farkas, J.B. Foresman, D.J. Fox, Gaussian, Inc., Wallingford CT, **2016**.

[34] N.M. O'Boyle, A.L. Tenderholt, K.M. Langner, *J. Comput. Chem.,* **2008**, *29,* 839–845.

How to cite this manuscript: Mohammad Reza Jalali Sarvestani, Zohreh Doroudi. Nalidixic Acid Adsorption on the Surface of Boron Nitride Nanocluster ($B_{12}N_{12}$): DFT Studies*, Adv. J. Chem. A*, **2020**, *3*, S740–S749.